Multiple Crashworthiness Evaluation of Double-V NPR Filled Square Tube under Axial impact

Huiming Sun[a,b], Hanting Zhou[c,b], Jiangfan Zhang [a], Liangmo Wang[a], Tao Wang[a]

a School of Mechanical Engineering, Nanjing University of Science and Technology Nanjing, Jiangsu, 210094, China

b School of Engineering, Lancaster University, Lancaster, Lancashire, LA1 4YW, UK

c School of economics and management, Nanjing University of Science and Technology, Nanjing, 210094, China

Abstract

Thin-walled structures are used extensively in the passive safety of vehicles to absorb energy. The thin-walled tube is already a traditional structure with excellent energy absorption. Negative Poisson's ratio (NPR) structures produce an inward concentration to increase the stiffness of the structure during axial compression. The concept of fluctuation of crushing force (*FoCF*) is introduced in this paper to evaluate this new energy absorbing box as an energy absorbing device based on the traditional energy absorption evaluation index. Based on experimental validation, a finite element model has been developed that can accurately predict the crashworthiness of the double-V NPR-filled square tube (DVFST). The following parameters, such as out-of-plane thickness meta cell half-width beam thickness beam angle tube thickness were carried out to assess the crashworthiness of the DVFST structure. The first thing that should be considered in the design of a DVFST structure is the half-width of the cell, followed by the angle of the long beam and then the relative wall thickness of the long and short beams. The DVFST structure has the potential to become an excellent energy-absorbing device by adjusting its parameters.

1 Introduction

With the application of autonomous driving technology, a vehicle with significant quality in terms of crashworthiness is a growing concern. Crashworthiness refers to the ability of the structure to absorb and convert excessive energy into plastic strain [1]. The superior performance of crashworthiness on vehicles can reduce the death and injury risk of the occupants in case of collision [2]. Thus, a good crashworthiness design has become a major safety standard for occupants-carrying vehicles. A wide variety of thin-walled tubular components have been developed for use in energy-absorbing structures to improve the crashworthiness performance of a structure [3]. According to a review of the available literature, structural geometry, materials, and loading mode are the principal factors that affect the energy absorption capability of the thin-walled tubular components [1, 3, 4].

The ability of thin-walled structures to absorb energy has been demonstrated in numerous types of research. Traditional cell tubular structures, consisting of a square, rectangular, circular, triangular, top-hat, double top-hat, w-shaped, tapered/conical, and polygonal cross-sections, have been widely used in thin-

walled structures with high crashworthiness [2, 5, 6]. Generally, square and circular thin-walled tubes are preferred in terms of energy absorption under impact loading due to their excellent crashworthiness characteristics, low economic costs, convenience, and accessibility [7, 8]. As structure complexity and crashworthiness requirements increase, hybrid structures with simple configurations are becoming the focus of research. Filling thin-walled tubes with aluminum foam can be a more effective method, as the interaction between the tube and foam can absorb additional energy [9-11]. Experiments show that auxetic structures with negative Poisson's ratio (NPR) property display anomalous expansions and contractions along the transverse direction when compressed and stretched [12]. Recently, it has been used as novel-filled thin and thick-walled materials [13, 14]. Further analysis with the fixed slenderness ratio finds that hybrid structures with double-arrowed auxetic (DAA) NPR as the filler could enhance crash energy absorption [15].

Material types for constructing thin-walled energy absorbers can be categorized into three types: metal/alloys, composites, and hybrid of composite-metal/alloys [16]. Among the metal/alloy categories, studies have mainly focused on steel and aluminum, such as aluminum alloy and mild steel. Reyes et al. [17] report that steel is normally chosen as the filler material due to its accessibility and cost efficiency, which has widely used in vehicle body constructions. As a lightweight yet strong material, aluminum alloy as a filler has been verified to increase the ability to absorb energy in either single or double wall conditions [18]. In contrast, composite materials are becoming increasingly popular in crashworthiness applications due to their high specific strength, stiffness, and energy absorption properties. In light of the strain rate effect of composite materials, thin-walled structures are susceptible to brittle fracture rather than ductile damage [19]. The composite structures absorb a greater amount of energy per unit mass (*SEA*) than the metallic structures. It must be noted, however, that it is difficult to recycle used composite materials and design composite structures because of their anisotropic material properties [20]. In addition, the manufacturing cost of composite materials is relatively higher than that of metallic structures, which has restricted their application [2]. Absorbers designed from renewable materials and wood-based composites meeting the criteria of a circular economy may be a good optional alternative in the future [21, 22]. Also, hybrid structures of composite-metal/alloys gain much more attention. Hybrid structures combined with desirable properties of material and composites, with the advantage of high strength, ductility, and stability, can absorb a greater amount of energy [23]. As metallic structures are widely used as energy absorbers in the vehicle body, this paper focuses on the metallic materials in thin-walled tubes to analyze the energy absorption behavior.

The concept of fluctuation of crushing force (*FoCF*) is introduced in this paper to evaluate this new energy absorbing box as an energy absorbing device based on the traditional energy absorption evaluation index. This article contains the following main sections: First, the structure of double-V NPR-filled square tube (DVFST) is described; the next is an introduction to finite element modelling; and then is the

description of model validation tests and crashworthiness evaluation indicators; finally, the parametric analysis of DVFST are conducted regarding evaluation index.

2 Structure and methodology

2.1 Structural Description

A host of re*SEA*rchers applied aluminum foam and common honeycomb as the filler of thin-walled tubes. In this paper, a novel tube structure is presented to improve the energy absorption performance, which is composed of the thin-walled square tube in Fig.1(a). and Double-V NPR structure in Fig.1(b). Its geometry is shown in Fig.1(c).

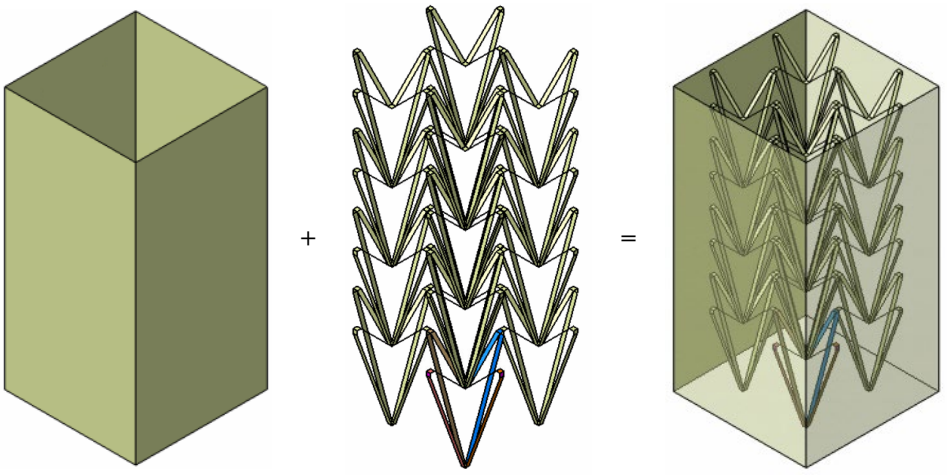

(a) Square Tube (b) Double-V NPR (c) DVFST

Fig.1 DVFST structure

The parameters of DVFST mainly include tube width W, tube height H, and tube thickness T. As is shown in Fig2, the parameters of the double-V NPR structure include the meta cell half-width L, the short beam angle θ_1, the long beam angle θ_2, the short beam thickness T_1, the long beam thickness T_2, and the effective height of a single meta cell he. The number of cells of the double-V NPR structure in the X/Y-axis direction is the same, and the number of cells in the Z-axis direction is determined by the height of the tube.

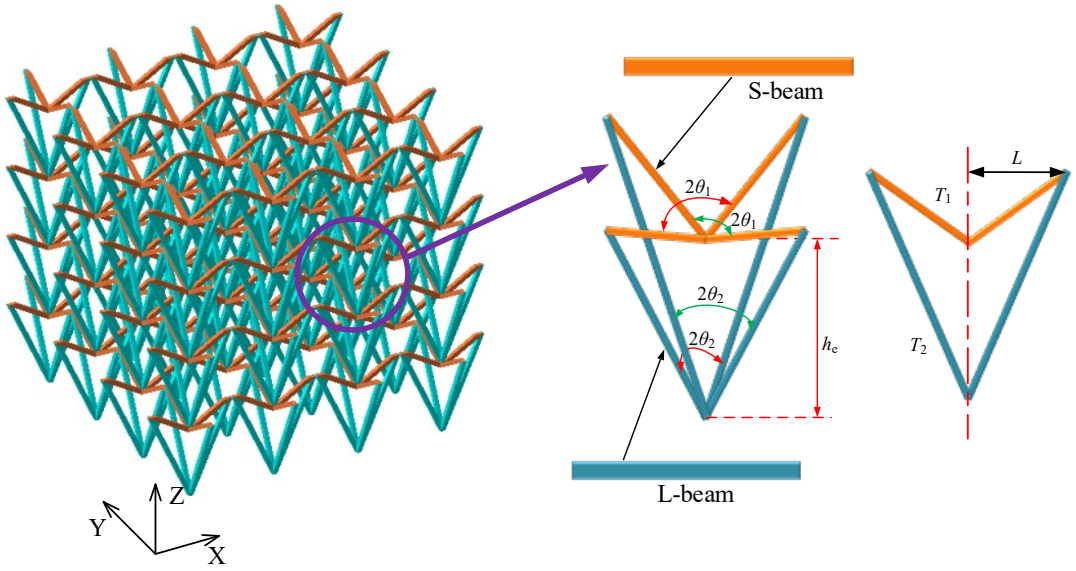

Fig.2 Schematic diagram of the three-dimensional NPR-filled core

2.2 Finite element models

In this study, the simulations of the validated model were carried out by non-linear finite element software Abaqus. All the models are made of AlSi10Mg with density ρ=2700kg/m^3, Young's modulus E=70GPa, initial yield stress=152MPa, ultimate strength=234MPa, and Poisson's ratio υ=0.3. Material properties for DVFST structure are shown in Fig3. The tube and cell wall mesh with shell elements (type S4R). Five integral points are set in the direction of shell element thickness to ensure the accuracy of the calculation. Fig4 illustrates the grid sensitivity analysis for tube and NPR. The grid sizes for tube are 2mm, 1mm, 0.75mm 0.5mm and for NPR 1mm, 0.75mm, 0.5mm, 0.25mm. Convergence is judged on the basis that the adjacent difference is less than 5%. The convergency test shows a suitable element size of 1mm for the tube and 0.5mm for the filled core. The bottom of the tube is constrained with all freedoms and the top is impacted with a rigid wall to simulate axial impact loading [24]. To simulate the self-contact of the structures themselves and mutual contact, 'General Contact' algorithms are employed. Both the static and dynamic friction coefficients are set as 0.2 and 0.3 [25, 26]. The impact velocity is 10m/s.

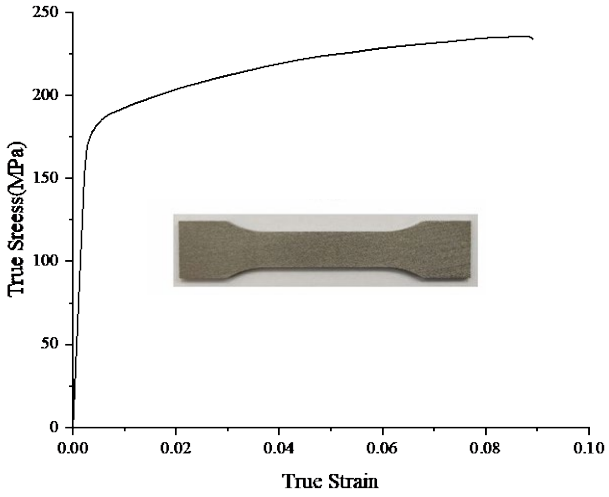

Fig.3 Material properties for DVFST structure

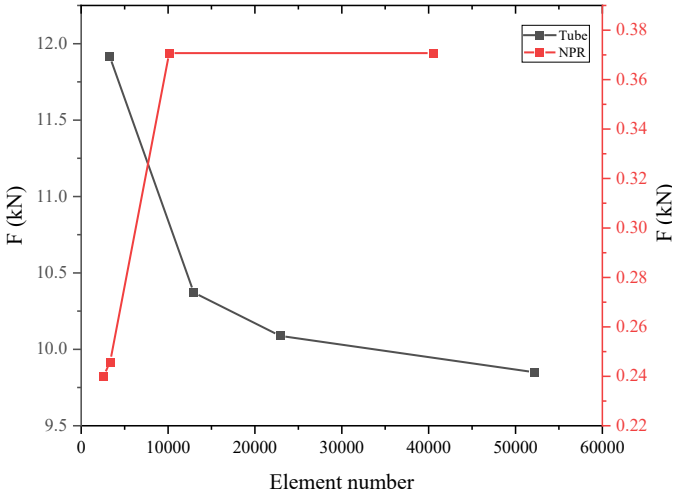

Fig.4 Grid sensitivity analysis for tube and NPR

2.3 Experiment

As shown in Fig.5. The experimental prototype of DVFST was made by additive manufacturing. During the process, an input power of 370 W, a scan speed of 1300 m/s, and a spacing between scan tracks of 190μm AlSi10Mg powders were supplied by EOS GmbH Electro Optical Systems. The thickness of each powder layer was set as 30μm in the printing direction. The prototypes were also performed at 250°C for four hours to relieve the stress.

(a) Tube (b) Double-V NPR (c) DVFST Structure

Fig.5. Experimental prototype made by additive manufacturing

Table 1 summarizes the geometric parameters of the DVFST experimental prototype.

Tab.1 Geometric parameters of DVFST

Parameters	Values	Parameters	Values
W	40mm	Y	2
T	1mm	Z	4
H	77mm	θ_1	45°
L	9.25mm	θ_2	20°
B	1mm	T_1	1mm
X	2	T_2	1mm

The quasi-static compression test was conducted to validate the FE model. The electronic universal testing machine CSS-44200 was employed. The force and displacement can be recorded with the equipped sensors whose error can be controlled by less than 0.5%. The maximum force can reach 200kN. The compression / tensile speed is continuously viable from 0.01 mm/min to 500 mm/min. The prototype is placed on the bottom plate and the top plate compresses downwards at a speed of 3 mm/min.

2.4 Evaluation index of structural crashworthiness

Usually, the total energy absorption (*EA*), peak crush force (*PCF*), mean crush force (*MCF*), specific energy absorption (*SEA*), crush force efficiency (*CFE*), and fluctuation of Crushing Force (*FoCF*) are considered to investigate the crushing response of DVFST. These indicators can be obtained and derived from the force-displacement responses of the DVFST. *PCF* values are the maximum force in the force-displacement graph and the structural design [25].

The *EA* is defined as the total energy absorption during the crushing displacement, which can be expressed as:

$$EA = \int_0^{d_{\max}} F(x)dx \tag{1}$$

Where the $d_{\max}$ is the maximum crushing length and $F(x)$ is the instantaneous force throughout the displacement x.

The *MCF* is calculated by dividing the *EA* by the crushing length and can be given by:

$$MCF = \frac{EA}{x} \tag{2}$$

The *SEA* is defined as the ratio of total energy absorption to the total mass of the DAFT and can be calculated as follows:

$$SEA = \frac{EA}{M} \tag{3}$$

Where the *M* is the total mass of the structure.

The *CFE* can be defined as *MCF* divided by *PCF*:

$$CFE = \frac{MCF}{PCF} \tag{4}$$

The standard deviation is the arithmetic mean of the squared deviation from the mean and reflects the degree of dispersion of a data set. Here we use the standard deviation to measure the deviation of the crushing force from the *MCF* during compression to evaluate the stability of thin-walled filled structures during impact. The *FoCF* is defined as the standard deviation of crushing force:

$$FoCF = \sigma(F) = sqrt(((F_1 - MCF)^2 + (F_2 - MCF)^2 + ...(F_n - MCF)^2)/n) \tag{5}$$

For each structure, the higher *EA*, *MCF*, *SEA,* and *CFE*, and the lower *PCF* and *FoCF* indicators are, the better the energy absorption capacity is.

2.5 Description of benchmark model parameters

Geometrical parameters have a strong influence on the crashworthiness of a structure. A parametric analysis of the crashworthiness of the DVFST structure is presented. The DVFST structural base model parameters are, n_X=n_Y=3, n_Z=7, *L*=6.17mm, B=2mm, θ_1=45°, θ_2=20°, T_1=1mm, T_2=1mm, *T*=1mm, the total height is 85mm. The overall height is maintained at 85 mm by adjusting the number of cells in the Z-direction for each parameter change.

3 Results and discussion

3.1 Finite element model validation

The force-displacement curve was captured as shown in Fig.6(b). The force-displacement curve predicted by the FE model with the same boundary conditions is plotted. The *PCF* values of experimental and FEA are 24.77kN and 26.96kN, respectively. The *MCF* values of experimental and FEA are 6.65kN and 7.02kN, respectively. It can be easy to calculate the relative error of *PCF* and *MCF* are 8.12% and 5.27%. Although, the initial fold deformation in the experiment is larger compared to the simulation, resulting in a backward shift of the second *PCF* in the experiment. However, this does not affect the trend of the compression force during compression, as the subsequent study of the manuscript is mainly focused on the compression force during compression. This illustrates the FE model is accurate to predict the mechanical properties of the DVFST [27, 28].

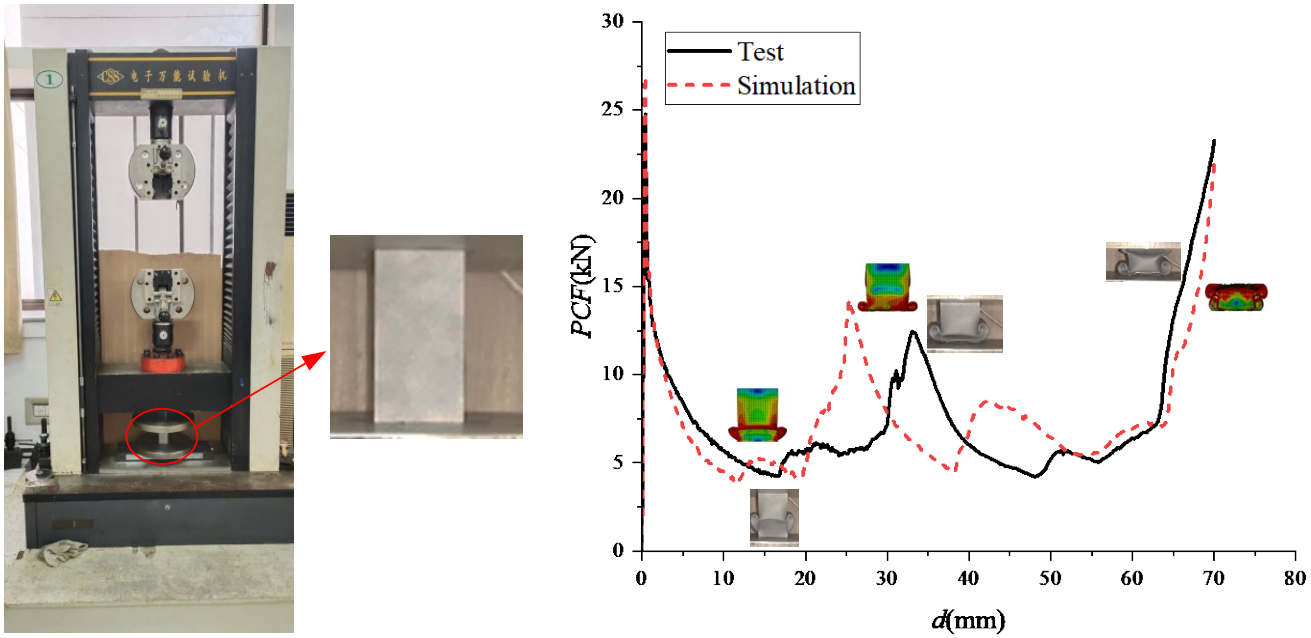

(a) Quasi-static testing of prototypes (b) Force-displacement curves and Deformation patterns

Fig. 6 Quasi-static compression test of the DVFST

3.2 Effects of out-of-plane thickness

The out-of-plane thickness variation parameters of the filled core are shown in Table 2.

Tab.2 Table of out-of-plane thickness variation parameters of filled core

	n_X	n_Y	n_Z	L/mm	B/mm	θ_1/°	θ_2/°	T_1/mm	T_2/mm	T/mm	m/g
B1	3	3	7	6.17	1	45	20	1.0	1.0	1.0	54.60
B2	3	3	7	6.17	2	45	20	1.0	1.0	1.0	66.30
B3	3	3	8	6.17	3	45	20	1.0	1.0	1.0	86.00
B4	3	3	9	6.17	4	45	20	1.0	1.0	1.0	104.90
B5	3	3	10	6.17	5	45	20	1.0	1.0	1.0	122.20

The out-of-plane thickness can significantly improve the relative density of the filled structure. As Shown in Fig7-9, an increase in the out-of-plane thickness results in a substantial advance in the densification strain of the structure. The *PCF* increases dramatically when the thickness increases to 4mm and 5mm in the out-of-plane. So, the *CFE* tends to increase and then decrease, with a maximum of 58% achieved in the out-of-plane direction at a thickness of 4mm. *FoCF* is more consistent with *PCF* changes. Compared to the FoCF of the structure at 2 mm in the out-of-plane direction, the FoFC increases by 10.60% when the thickness in the out-of-plane direction is 4 mm and by 25.82% when the thickness in the out-of-plane direction is 5 mm. At compression distances of less than 30 mm, a smaller thickness in the out-of-plane direction results in a larger *SEA*. As the impact distance increases, the state of the *SEA* begins to diverge, as shown by the fact that those with a thickness of 1mm show a lack of back strength, while the rest maintain a strong tendency to increase, with the three structures with a greater thickness leading to a sharp increase in *SEA* as they enter the densification phase. Taking the above analysis into account, the ideal outside the face thickness is around 4mm.

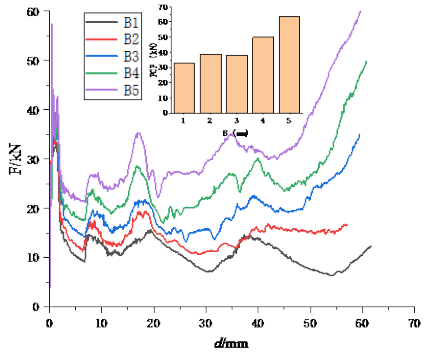

Fig7 The effect of out-of-plane thickness on *F* and *PCF*

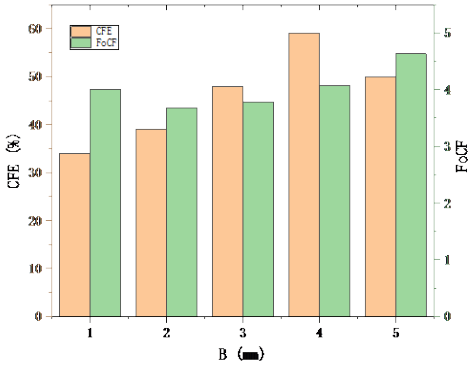

Fig8 The effect of out-of-plane thickness on *CFE* and *FoCF*

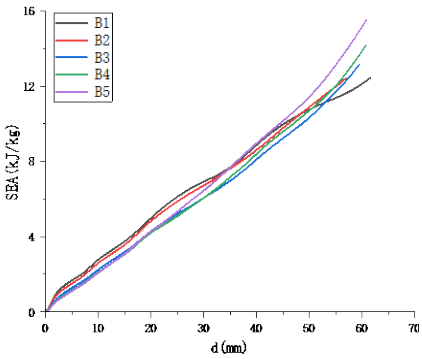

Fig9 The effect of out-of-plane thickness on *SEA*

3.3 Effects of meta cell half-width

The meta cell half-width variation parameters of the filled-core are shown in Table 3.

Tab.3 Table of meta cell half-width variation parameters of filled core

	n_X	n_Y	n_Z	L/mm	B/mm	θ_1/°	θ_2/°	T_1/mm	T_2/mm	T/mm	m/g
XY2	**2**	**2**	5	**9.25**	2	45	20	1.0	1.0	1.0	53.92
XY3	**3**	**3**	7	**6.17**	2	45	20	1.0	1.0	1.0	66.30
XY4	**4**	**4**	10	**4.63**	2	45	20	1.0	1.0	1.0	93.61
XY5	**5**	**5**	12	**3.70**	2	45	20	1.0	1.0	1.0	115.70
XY6	**6**	**6**	15	**3.08**	2	45	20	1.0	1.0	1.0	150.12

The meta cell half-width variation can also increase the relative density of the filled structure. As the number of cells in the XY direction increases, the half-width of the cells decreases, and the number of cells filling the space increases. Since the half-width of a cell is an integer, the half-width is adjusted to suit the number of cells in the XY direction. At the same time, the overall height of the structure was adjusted to around 85 mm by adjusting the number of vertical cells.

As is shown in Fig.10, the *PCF* increases as the cell half-width decreases, due to the stiffening of the structure because of the increased relative density of the filled structure. For the same problem, the densification strain of the structure is advanced due to the increase in the number of cells filled. From the fig 11, it can be found that the *CFE* increases significantly as the number of cells increases, indicating that the filled core has a significant effect on the improvement of the structural impact resistance. At the same time, the *FoCF* is not particularly sensitive to changes in the number of cells in the XY direction. The trend in *SEA* can be seen in Fig.12, where the difference in *SEA* is not very pronounced when the number of cells in the XY direction is 2, 3, and 4. When the number of cells is 5 and 6, the *SEA* of the structure is greatly increased concerning the previous parameters. In summary, the XY direction is a good choice for a meta cell number of 5, which balances the evaluation metrics.

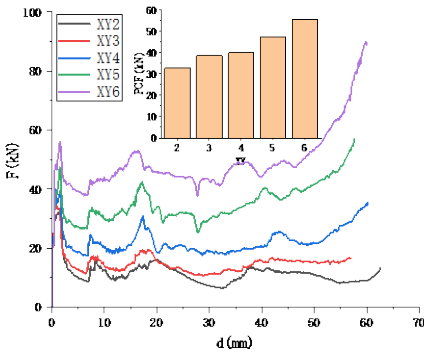

Fig10 The effect of meta cell half-width on *F* and *PCF*

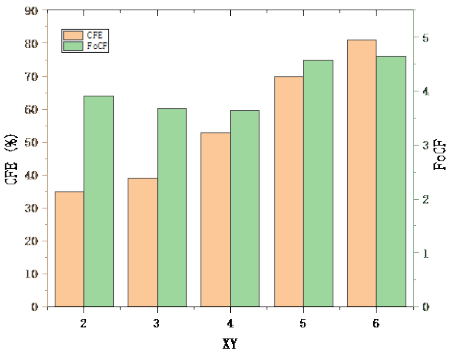

Fig11 The effect of meta cell half-width on *CFE* and *FoCF*

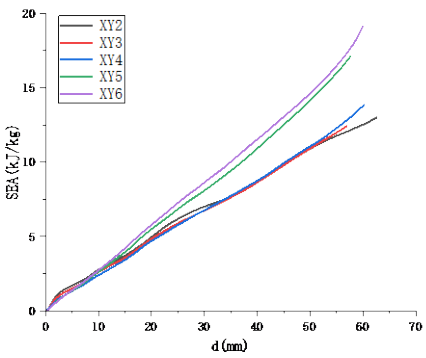

Fig12 The effect of meta cell half-width on *SEA*

3.4 Effects of the beam thickness

The thickness of the long and short beams of a structure can greatly influence the crashworthiness of the structure. The discussion of the variation in the thickness of the long and short beams is divided into three cases: 1) fixing the wall thickness of the short beam at 1mm and observing the effect of the variation in the thickness of the long beam on the crashworthiness; 2) fixing the wall thickness of the long beam at 1mm and observing the effect of the variation in the thickness of the short beam on the crashworthiness; 3) the difference in the crashworthiness of the structure when the long and short beams are varied simultaneously. The beam thickness variation parameters of the filled core are shown in Table 4.

Tab.4 Table of Effects of the beam thickness variation parameters of filled-core

No.	n_X	n_Y	n_Z	L/mm	B/mm	θ_1/°	θ_2/°	T_1/mm	T_2/mm	T/mm	m/g
1	3	3	7	6.20	2	45	20	1	**0.8**	1.0	61.60
2	3	3	7	6.17	2	45	20	1	**1**	1.0	66.30
3	3	3	7	6.13	2	45	20	1	**1.2**	1.0	70.90
4	3	3	7	6.10	2	45	20	1	**1.4**	1.0	75.40
5	3	3	7	6.07	2	45	20	1	**1.6**	1.0	79.90
6	3	3	7	6.17	2	45	20	**0.8**	1	1.0	63.70
7	3	3	7	6.17	2	45	20	**1**	1	1.0	66.30
8	3	3	7	6.17	2	45	20	**1.2**	1	1.0	68.90
9	3	3	7	6.17	2	45	20	**1.4**	1	1.0	76.50
10	3	3	7	6.17	2	45	20	**1.6**	1	1.0	81.60
11	3	3	7	6.20	2	45	20	**0.8**	**0.8**	1.0	59.10
12	3	3	7	6.17	2	45	20	**1**	**1**	1.0	66.30
13	3	3	7	6.13	2	45	20	**1.2**	**1.2**	1.0	73.50
14	3	3	7	6.10	2	45	20	**1.4**	**1.4**	1.0	80.60
15	3	3	7	6.07	2	45	20	**1.6**	**1.6**	1.0	87.70

From Figure 13, the *PCF* fluctuates relatively little for long beams less than 1.6mm thick, with a rise in the *PCF* when the maximum thickness of the long beam is achieved. In contrast, Figure 14 shows that the *CFE* at this point decreases significantly with the long beam thicknesses of 1.2mm and 1.4mm. Combined with the *SEA* results in Figure 15, it is easy to see that when the thickness of the long beam is slightly greater than the thickness of the short beam, the structure can achieve good crashworthiness, by maintaining the relative thickness of the long and short beams is important in the design. This can be explained by the fact that during compression in the axial direction, flexure occurs in long beams subjected to compression, while

short beams behave mainly in tension. When the thickness of the long beam is less than or equal to that of the short beam, the premature buckling of the long beam affects the deformation of the short beam, which reduces the energy absorption of the structure. As the thickness of the long beam continues to increase, the stiffness of the long and short beams tend to be in relative equilibrium, which allows both to deform sufficiently to absorb energy. However, as the thickness of the long beam increases further, the overall weight of the structure rises and not only does the PCF of the structure increase significantly but also the SEA decreases. A ratio of 1.2 to 1.4 between the long and short beams gives better crashworthiness.

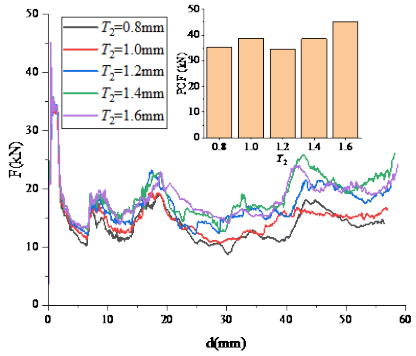

Fig13 The effect of long beam thickness varies on *F* and *PCF*

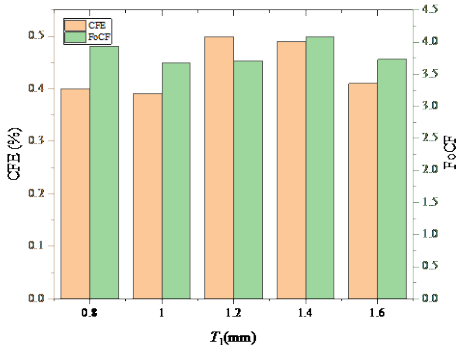

Fig14 The effect of long beam thickness varies on *CFE* and *FoCF*

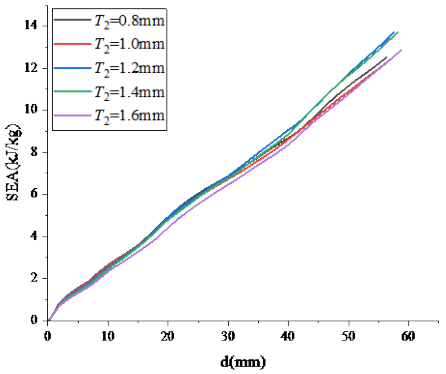

Fig15 The effect of long beam thickness varies on *SEA*

As can be seen from Figure 16, the *PCF* is less sensitive to changes in the thickness of the short beam. The *PCF* achieves a maximum value when the long and short beam thicknesses are the same, Figure 17 which corresponds to the lowest *CFE* as well as the largest *FoCF*. Figure 18 clearly shows that an increase in the thickness of the short beam inhibits the growth of the *SEA* and that a thinner short beam thickness should be adopted in the design to improve the *SEA* of the structure.

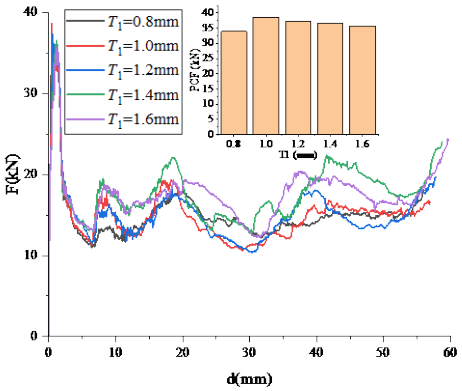

Fig16 The effect of short beam thickness varies on *F* and *PCF*

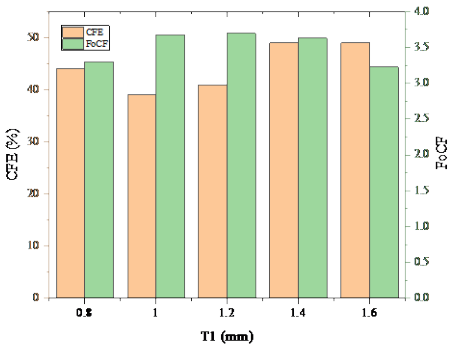

Fig17 The effect of short beam thickness varies on *CFE* and *FoCF*

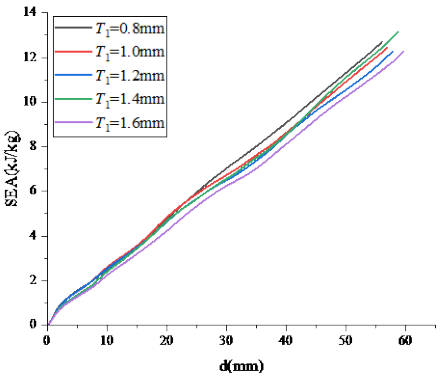

Fig18 The effect of short beam thickness varies on *SEA*

As can be seen in Figure 19, the *PCF* increases and then decreases as the length of the beam increases simultaneously, achieving a maximum value of 43.15kN at 1.2 mm. This is exactly the opposite of the trend in the *CFE* (Figure 20). When the thickness is 1mm, the structure has a minimum *FoCF* of 3.68, which corresponds to the smallest variation in the crushing force of the structure. From Figure 21, the difference in

SEA is not large but shows a general upward trend.

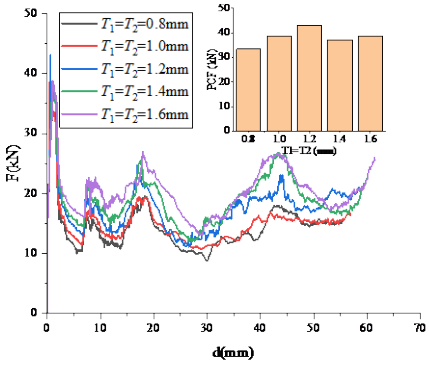

Fig19 The effect of thickness beams varies simultaneously on *F* and *PCF*

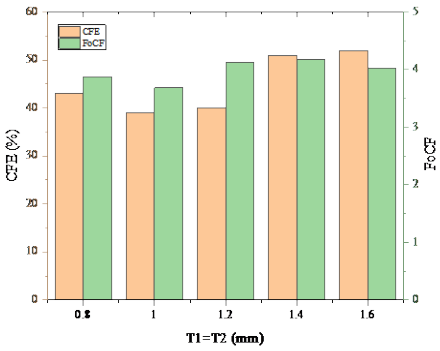

Fig20 The effect of beams thickness varies simultaneously on *CFE* and *FoCF*

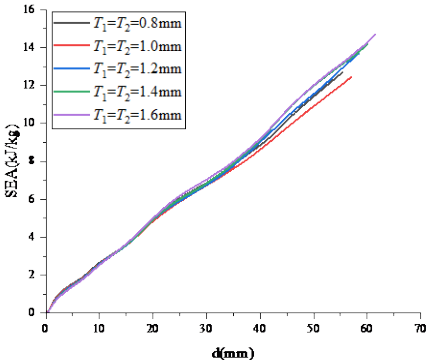

Fig21 The effect of beams thickness varies simultaneously on *SEA*

3.5 Effects of the beam angle

The beam angle variation parameters of the filled core are shown in Table 5.

Tab.5 Table of Effects of the beam angle variation parameters of filled-core

No.	n_X	n_Y	n_Z	L/mm	B/mm	θ_1/°	θ_2/°	T_1/mm	T_2/mm	T/mm	m/g
1	3	3	5	6.20	2	45	**15**	1	1	1.0	63.40
2	3	3	7	6.17	2	45	**20**	1	1	1.0	66.30
3	3	3	10	6.13	2	45	**25**	1	1	1.0	75.00
4	3	3	14	6.10	2	45	**30**	1	1	1.0	86.50
5	3	3	19	6.07	2	45	**35**	1	1	1.0	99.00
6	3	3	8	6.17	2	**40**	20	1	1	1.0	74.00
7	3	3	7	6.17	2	**45**	20	1	1	1.0	66.30
8	3	3	7	6.17	2	**50**	20	1	1	1.0	67.40
9	3	3	7	6.17	2	**55**	20	1	1	1.0	68.30
10	3	3	6	6.17	2	**60**	20	1	1	1.0	59.70

As shown in Figures 22 and 23, the *PCF* of the structure tends to decrease as the angle of the long beams increases, since the increase in the angle of the long beams causes the metamorphic cells to be prone to plastic collapse. At the same time, the *CFE* of the structure shows an increasing trend due to the increase in relative density. At a long beam angle of 35°, the *FoCF* changes drastically from the previous values. As can be seen in Figure 24, the *SEA* of the structure decreases as the angle of the long beam increases, where the *SEA* of the structure is superior at a long beam angle of 20°.

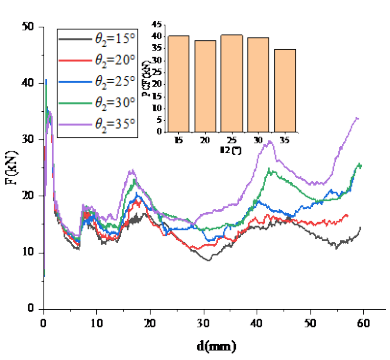

Fig22 The effect of long beam angle varies on *F* and *PCF*

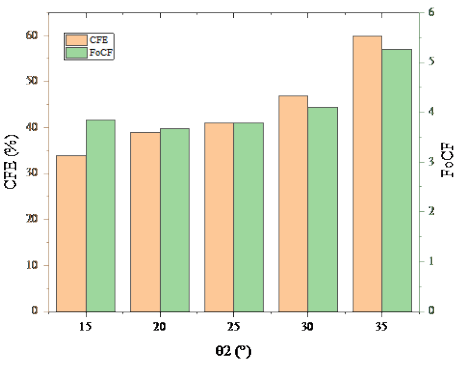

Fig23 The effect of long beam angle varies on *CFE* and *FoCF*

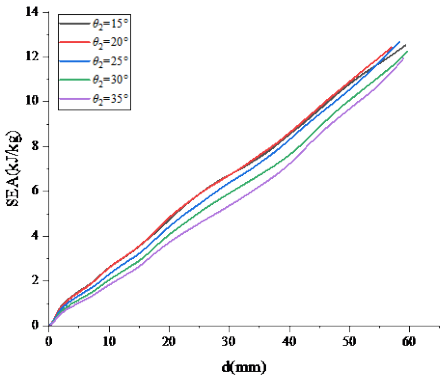

Fig24 The effect of long beam angle varies on *SEA*

As can be seen from Figures 25 and 26, the *PCF* of the structure fluctuates within a small range as the angle of the short beam increases, with the *CFE* showing a downward trend and the *FoCF* showing a steady trend, indicating that the *FoCF* is not sensitive to changes in the angle of the short beam. In contrast to the effect of the long beam angle on the *SEA*, an increase in the short beam angle causes the *SEA* to fluctuate in the form of an increase, then a decrease, and then an increase (Figure 27).

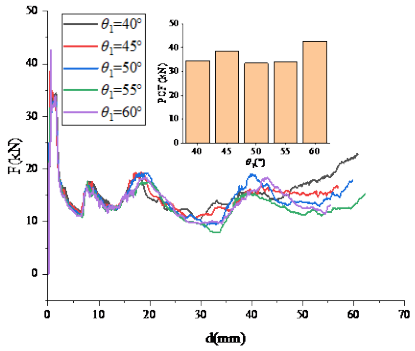

Fig25 The effect of short beam angle varies on *F* and *PCF*

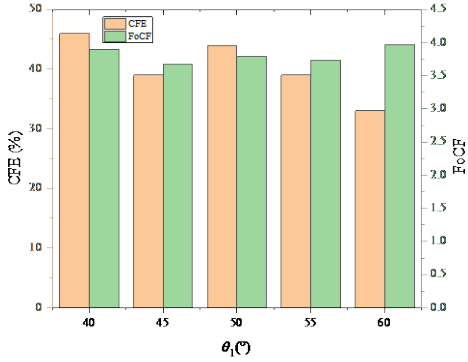

Fig26 The effect of short beam angle varies on *CFE* and *FoCF*

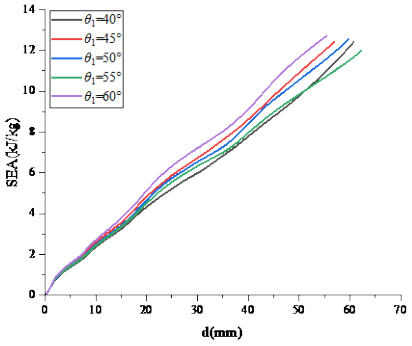

Fig27 The effect of short beam angle varies on *SEA*

3.6 Effects of the tube thickness

The tube thickness variation parameters of the filled core are shown in Table 6.

Tab.6 Table of effects of the tube thickness variation parameters of filled core

No.	n_X	n_Y	n_Z	L/mm	B/mm	θ_1/°	θ_2/°	T_1/mm	T_2/mm	T/mm	m/g
1	3	3	7	6.23	2	45	20	1	1	**0.8**	60.21
2	3	3	7	6.17	2	45	20	1	1	**1**	66.30
3	3	3	7	6.10	2	45	20	1	1	**1.2**	72.20
4	3	3	7	6.03	2	45	20	1	1	**1.4**	77.80
5	3	3	7	5.97	2	45	20	1	1	**1.6**	83.30

As is shown in Fig.28 to Fig.30, with the increase of the tube thickness, all crashworthiness indicators also simultaneously increase. The thicker the wall thickness of the square tube, the greater the *PCF* and *SEA* of the structure will increase, but at the same time exhibit a greater degree of load fluctuation. It is necessary to choose a relative wall thickness that is appropriate to the filled core.

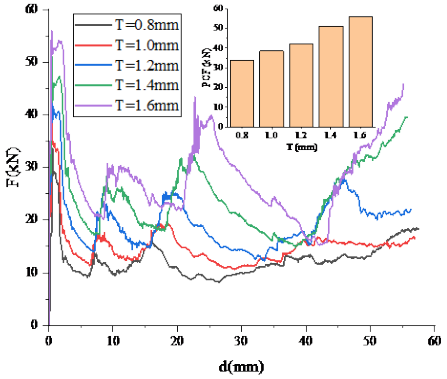

Fig.28 The effect of tube thickness varies on *F* and *PCF*

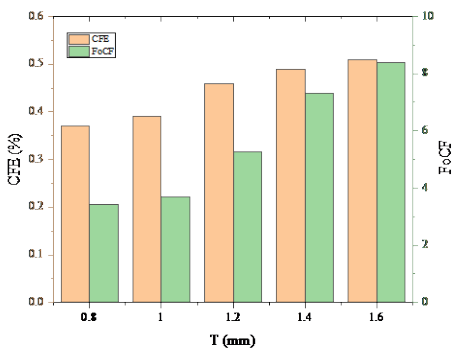

Fig.29 The effect of tube thickness varies on *CFE* and *FoCF*

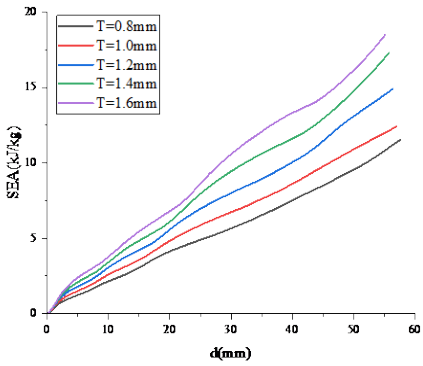

Fig.30 The effect of tube thickness varies on *SEA*

4 Conclusions

In this paper, multiple crashworthiness evaluation of DVFST structure was analyzed. This paper introduces *FoCF* as an evaluation indicator to enrich the evaluation dimension of the structure during the crushing process. The results show that by adjusting the structural parameters, the DVFST structure can be made more crashworthy. Through the parametric analysis of DVFST, we can conclude the following:

1. A reasonable selection of thicknesses in the out-of-plane direction can significantly improve the *CFE* and *SEA* of the structure with a small uplift in *PCF* and *FoCF*. The *CFE* tends to increase and then decrease, with a maximum of 58% achieved in the out-of-plane direction at a thickness of 4mm. Compared to the *FoCF* of the structure at 2 mm in the out-of-plane direction, the *FoFC* increases by 10.60% when the thickness in the out-of-plane direction is 4 mm and by 25.82% when the thickness in the out-of-plane direction is 5 mm. The ideal outside the face thickness is around 4mm.

2. A suitable choice of cell half-width is important to obtain a high *CFE* and *SEA* where *PCF* and *FoCF* are acceptable. A reasonable number of cells for analysis in this paper is 5 in each XY direction.

3. A thinner short beam thickness should be adopted in the design to improve the *SEA* of the structure. The relative thickness of the long and short beams is important, and analysis shows that a ratio of 1.2 to 1.4 between the long and short beams gives better crashworthiness.

4. Crashworthiness parameters are more sensitive to changes in the angle of long beams than to changes in the angle of short beams. It is necessary to choose a relative wall thickness that is appropriate to the filled core.

The first thing that should be considered in the design of a DVFST structure is the half-width of the cell, followed by the angle of the long beam and then the relative wall thickness of the long and short beams. The thickness of the inner core in the out-of-plane direction and the wall thickness of the tube can use to adjust the relative stiffness of the tube and the inner core to obtain a greater energy absorption capacity. This paper can be used as a basis for the optimization of DVFST and its extension to multi-cell thin-walled tubes in the future.

References

[1] Abada, M. and A. Ibrahim, *Hybrid multi-cell thin-walled tubes for energy absorption applications: Blast shielding and crashworthiness.* Composites Part B: Engineering, 2020. **183**: p. 107720.

[2] Baroutaji, A., M. Sajjia, and A.-G. Olabi, *On the crashworthiness performance of thin-walled energy absorbers: recent advances and future developments.* Thin-Walled Structures, 2017. **118**: p. 137-163.

[3] Gao, Q. and W.-H. Liao, *Energy absorption of thin walled tube filled with gradient auxetic structures-theory and simulation.* International Journal of Mechanical Sciences, 2021. **201**: p. 106475.

[4] Wang, Z., et al., *Matching effect of honeycomb-filled thin-walled square tube—experiment and simulation.* Composite Structures, 2016. **157**: p. 494-505.

[5] Nia, A.A. and J.H. Hamedani, *Comparative analysis of energy absorption and deformations of thin walled tubes with various section geometries.* Thin-Walled Structures, 2010. **48**(12): p. 946-954.

[6] Chen, B., et al., *Experimental study on energy absorption of bionic tubes inspired by bamboo structures under axial crushing.* International Journal of Impact Engineering, 2018. **115**: p. 48-57.

[7] Ming, S., et al., *Energy absorption of thin-walled square tubes designed by kirigami approach.* International Journal of Mechanical Sciences, 2019. **157**: p. 150-164.

[8] Li, R., J. Xiong, and Y. Lei, *Investigation on thermal stress evolution induced by wire and arc additive manufacturing for circular thin-walled parts.* Journal of Manufacturing Processes, 2019. **40**: p. 59-67.

[9] Li, Z., R. Chen, and F. Lu, *Comparative analysis of crashworthiness of empty and foam-filled thin-walled tubes.* Thin-Walled Structures, 2018. **124**: p. 343-349.

[10] Pozniak, A., J. Smardzewski, and K. Wojciechowski, *Computer simulations of auxetic foams in two dimensions.* Smart Materials and Structures, 2013. **22**(8): p. 084009.

[11] Wojciechowski, K., *Two-dimensional isotropic system with a negative Poisson ratio.* Physics Letters A, 1989. **137**(1-2): p. 60-64.

[12] Lakes, R., *Foam structures with a negative Poisson's ratio.* Science, 1987. **235**(4792): p. 1038-1040.

[13] Joseph, A., V. Mahesh, and D. Harursampath, *On the application of additive manufacturing methods for auxetic structures: A review.* Advances in Manufacturing, 2021. **9**(3): p. 342-368.

[14] Lin, S., et al., *A Design Framework for Negative Poisson's Ratio Structure with Curved Beam-Compliant Mechanism Unit Cells.* physica status solidi (b), 2022: p. 2100599.

[15] Gao, Q., et al., *Crashworthiness analysis of double-arrowed auxetic structure under axial impact loading.* Materials & Design, 2019. **161**: p. 22-34.

[16] Abdullah, N., et al., *A review on crashworthiness studies of crash box structure.* Thin-Walled Structures, 2020. **153**: p. 106795.

[17] Reyes, A. and T. Børvik, *Quasi-static behaviour of crash components with steel skins and polymer foam cores.* Materials Today Communications, 2018. **17**: p. 541-553.

[18] Wang, J., et al., *Crashworthiness behavior of Koch fractal structures.* Materials & Design, 2018. **144**: p. 229-244.

[19] Wang, K., et al., *On crashworthiness behaviors of 3D printed multi-cell filled thin-walled structures.* Engineering Structures, 2022. **254**: p. 113907.

[20] Shin, K.C., et al., *Axial crush and bending collapse of an aluminum/GFRP hybrid square tube and its energy absorption capability.* Composite structures, 2002. **57**(1-4): p. 279-287.

[21] Kciuk, S., G. Bienioszek, and E. Krzystała. *Analysis of dynamics of the blast mitigation seat*. in *International Scientific Conference Advances in Applied Biomechanics*. Wisla, Poland, 2020. Springer.

[22] Smardzewski, J., M. Maslej, and K.W. Wojciechowski, *Compression and low velocity impact response of wood-based sandwich panels with auxetic lattice core.* European Journal of Wood and Wood Products, 2021. **79**(4): p. 797-810.

[23] Kumar, A.P., D. Maneiah, and L.P. Sankar, *Improving the energy-absorbing properties of hybrid aluminum-composite tubes using nanofillers for crashworthiness applications.* Proceedings of the Institution of Mechanical Engineers, Part C: Journal of Mechanical Engineering Science, 2021. **235**(8): p. 1443-1454.

[24] Shen, G., X. Wang, and D. Li, *Mechanical Properties Analysis on a Novel Negative Poisson's Ratio Voronoi Foam-Filled Corrugated Tube Under Impact Loading.* physica status solidi (b), 2021. **258**(8): p. 2100128.

[25] Sun, G., et al., *Crashworthiness design for functionally graded foam-filled thin-walled structures.* Materials Science and

Engineering: A, 2010. **527**(7-8): p. 1911-1919.
[26] Zhou, G., et al., *Design optimization of a novel NPR crash box based on multi-objective genetic algorithm.* Structural and Multidisciplinary Optimization, 2016. **54**(3): p. 673-684.
[27] Magliaro, J. and W. Altenhof, *Analytical predictions of the complete mechanical response of AA6061 energy absorbers subjected to axial cutting.* Thin-Walled Structures, 2019. **139**: p. 151-168.
[28] Fu, M., et al., *Experimental and numerical analysis of a novel three-dimensional auxetic metamaterial.* physica status solidi (b), 2016. **253**(8): p. 1565-1575.

Acknowledgments

This work was supported by the National Natural Science and Foundation of China (Grant No.51975295), the National Natural Science and Foundation of China (Grant No. 52202444), the Natural Science Foundation of Jiangsu Province (Grant No. BK20190462), China Scholarship Council (CSC) (Grant No.202106840028).